Spectroscopy of barium $6p_{1/2}nk$ autoionizing states in a weak electric field

J. Nunkaew and T. F. Gallagher
Department of Physics, University of Virginia, Charlottesville, Virginia 22904, USA
(Received 28 February 2012; published 3 July 2012)

We have studied the Ba $6p_{1/2}nk$, $n = 17$, $5 \leqslant k \leqslant n-1$ Stark autoionizing states by isolated core excitation (ICE) of the Ba $6snk$ Stark bound states in very weak electric fields, an unexplored regime. In zero field the broad $\ell = 5$ state overlaps all the higher ℓ states, and in fields less than ~12 V/cm the Stark states composed of the $\ell > 5$ states are within the zero-field width of the nh state. In the ICE spectra the strongest transition from the $6snk$ Stark state is to the $6p_{1/2}nk$ Stark state, and shake-up satellite transitions are observed to higher-lying Stark states but not to lower-lying Stark states, a phenomenon which we attribute to the fact that the two Stark manifolds are both incomplete and different. The observed spectra can be described by treating the $6p_{1/2}nk$ Stark states, composed of the $\ell > 5$ states, as discrete states embedded in a continuum, the broad $6p_{1/2}nh$ state.

DOI: 10.1103/PhysRevA.86.013401 PACS number(s): 32.80.Zb, 32.60.+i, 32.30.Jc

I. INTRODUCTION

While the spectroscopy of autoionizing states in electric fields has been studied extensively [1–4], it has generally been carried out in relatively strong fields, in excess of 1 kV/cm, in which the Stark states are well separated and have widths greater than a typical laser linewidth of 0.1 cm^{-1}. While the major features of the observations can be understood with a simple, nearly hydrogenic model [5], detailed comparisons have required a more sophisticated quantum-defect-theory treatment [1]. In contrast, the spectroscopy of the Stark states composed of the nearly degenerate high-ℓ autoionizing states in the low-electric-field regime has never been explored. This regime is of practical importance in dielectronic recombination (DR) since only very low fields are required to convert the high-ℓ states into Stark states, which are linear superpositions of ℓ states. The low-ℓ character in each of the Stark states can endow it with enough autoionization rate to contribute to the DR rate, leading to an increase in the DR rate in even a small electric field [6–8]. Similarly, the conversion of molecular $n\ell$ Rydberg states into Stark states allows the optical excitation of long-lived Stark states, often termed zero electron kinetic energy (ZEKE) states, which have lifetimes orders of magnitude longer than the rapidly predissociating, optically accessible low-ℓ states [9,10].

Here we report the spectroscopy of the Ba $6p_{1/2}nk$ states of $n = 17$ in fields from 0 to 47 V/cm. In this regime the Stark states are composed primarily of the zero-field ℓ states of $\ell > 4$. A difference from the previous work is that the zero-field $6p_{1/2}17h$ state has a width of 10.5 GHz, which encompasses all the higher-ℓ states. In zero field they are not coupled, but when a field is present they are. We have used isolated core excitation (ICE) to drive atoms from the bound $6snk$ states to the autoionizing $6p_{1/2}nk$ states, a process in which the Ba^+ ion makes the $6s$-to-$6p$ transition, while the outer electron is a spectator [11]. Although there are exceptions, in most cases with ICE there is no excitation amplitude to the continuum, with the result that approximately Lorentzian lines are observed rather than the asymmetric Beutler-Fano profiles commonly seen with autoionizing states [12,13]. Due to the overlap of the broad $6p_{1/2}17h$ state with the Stark states composed of the higher-ℓ states there are two excitation amplitudes in this ICE, and we have treated the resulting line shapes with Fano's configuration interaction theory.

In the sections which follow we first outline the experimental approach. We then present the experimental data and discuss the incomplete Stark effect and overlap integrals which are used to calculate the excitation spectra from the Ba $6snk$ bound states to the $6p_{1/2}nk'$ autoionizing states. We present the observed autoionization widths as functions of electric field. Finally, we generate model spectra and compare them to the experimental data. Possible sources of the discrepancies between the observations and calculations are discussed. We use atomic units, unless specified otherwise.

II. EXPERIMENTAL APPROACH

As shown schematically in Fig. 1, Ba atoms from a heated oven are collimated into a 5-mm-diam beam, which passes between two copper plates 1.2 cm apart inside a vacuum chamber at a pressure of $\sim 10^{-7}$ Torr. The propagation directions of the Ba beam and laser beams are perpendicular to reduce the Doppler broadening. The bottom plate is connected to a positive high-voltage pulse to drive Ba ions resulting from autoionization to the MCP detector. The top plate is either grounded or connected to a Hewlett-Packard 8112A pulse generator which provides a negative voltage ramp.

The excitation scheme is shown by the energy-level diagram of Fig. 2(a). Ground-state Ba $6s^2\ {}^1S_0$ atoms are excited to the Ba $5d6p\ {}^1P_1$ state by a 350.211-nm 5-ns laser pulse which is produced by passing an amplified dye laser pulse of 700.422 nm through an angle-tuned frequency-doubling potassium dihydrogen phosphate (KDP) D″ crystal. Atoms in the Ba $5d6p\ {}^1P_1$ state are driven sequentially to the $6s5d\ {}^1D_2$ state, the $5d6p\ {}^1F_3$ state, and the $6sng\ {}^1G_4$ state by 582.789-, 648.47-, and ~674-nm 5-ns laser pulses, respectively. Laser excitation of the atoms occurs between the plates shown in Fig. 1 in a field of 40–60 V/cm, which expels ions produced by the absorption of a second 350-nm photon. Due to the large quantum defects of the $\ell \leqslant 4$ states, the Stark shifts of these ℓ states are negligible. There are two timing schemes used in this experiment, as shown Figs. 2(b) and 2(c). The timing scheme shown in Fig. 2(b) is used to observe the autoionizing spectra in low electric fields (fields less than 25 V/cm). In this scheme, the electric field of 40 V/cm is reduced to the desired

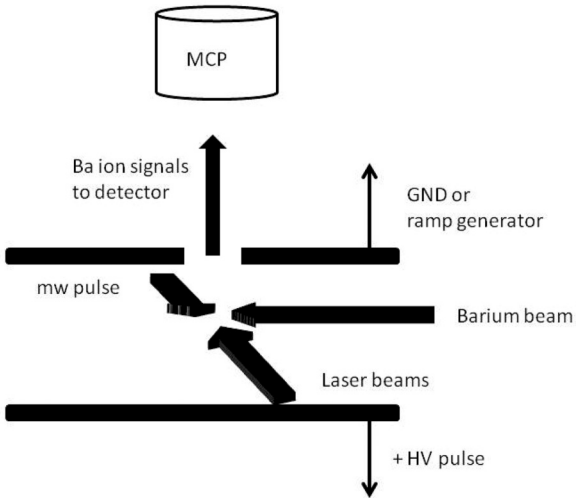

FIG. 1. Schematic diagram of the apparatus. The barium beam and laser beams are perpendicular. All the beams intersect in the interaction area between two plates. The ions are detected by the microchannel plate (MCP) detector placed above the hole in the top plate.

value in 250 ns. At a time 500 ns later, the microwave pulse is introduced into the interaction region to drive the atoms from the $6sng\ ^1G_4$ state to a $6snk$ Stark state of $k \geqslant 5$. Here k is the Stark quantum number, replacing ℓ. For $k > 4$ each k state is adiabatically connected to the zero-field state of $\ell = k$. The Stark states are linear combinations of zero-field $\ell > 4$ states, and the microwave transition from the $6sng$ state occurs via the $\ell = 5$ component of the $6snk$ state. For $E = 10$ V/cm the $6s17k$ Stark states are separated by ~100 MHz, and we are thus able to easily resolve the microwave transitions to different k states. The timing scheme shown in Fig. 2(c) is used to observe the autoionization widths of the autoionizing states as a function of electric field. In this scheme, the four lasers are fired in a field of 60 V/cm. At a time 500 ns after laser excitation a linear decrease of the field in time is started, and a 1-μs microwave pulse is introduced into the interaction region. The population transfer from $6sng$ to $6snk$ occurs by adiabatic rapid passage. The slew rate of the field pulse is varied to reach the desired field strength when the last laser is fired. The field strength can be reduced almost to zero while the atoms remain in the $6snk$ states. The timing scheme of Fig. 2(b) provides a very accurate absolute energy scale since the field strength and the microwave frequencies are fixed. However, in the near-zero-field regime population transfer by the method of Fig. 2(b) is small due to the small fraction of $\ell = 5$ component in the $6snk$ states. Hence, to observe the autoionization width in near-zero fields, we use the timing scheme of Fig. 2(c).

Atoms in the $6snk$ states are excited to the $6p_{1/2}nk'$ states by the last laser pulse of ~493.5 nm 100 and 500 ns after the microwave pulse for timing schemes of Figs. 2(b) and 2(c), respectively. Subsequent to ICE the doubly excited $6p_{1/2}nk'$ state quickly autoionizes, and the ions are collected 200 ns later by the positive high-voltage pulse. The high-voltage pulse drives both the Ba ions from autoionization and the ions photoionized by the first laser to the detector. However, due to the initial 40–60 V/cm field, the photoions produced by the first laser arrive at the MCP detector earlier than the ions from autoionization. The two signals can be distinguished in time, and we set a gate on the autoionization signal. The autoionization signal is recorded with a gated integrator as the wavelength of the 493-nm laser is slowly scanned across the $6snk$-$6p_{1/2}nk$ transition over many shots of the laser. The gated integrator signals are stored in a computer for later analysis.

The 5-ns laser pulse of ~493.5 nm is produced by a frequency-doubled, pulse-amplified 987-nm diode laser. The dye-amplified diode laser linewidth is ~300 MHz. To determine the absolute wavelength of the diode laser, we use an iodine absorption cell as the reference, and a Fabry-Perot interferometer of 1.5 GHz free-spectral range provides a relative frequency scale. A 10-cm-long iodine absorption cell is heated in a small oven to ~150 °C to increase the I_2 vapor pressure to 10–100 kPa. We use a photodiode to detect the 987-nm beam after retroreflection through the iodine absorption cell. As the master diode is scanned, the ir beam is absorbed at known transitions of iodine. We use the transition at 10130.9804 cm^{-1} as our frequency marker [14].

Microwaves in the 40–75-GHz frequency range are required in this experiment, and we generate them in the

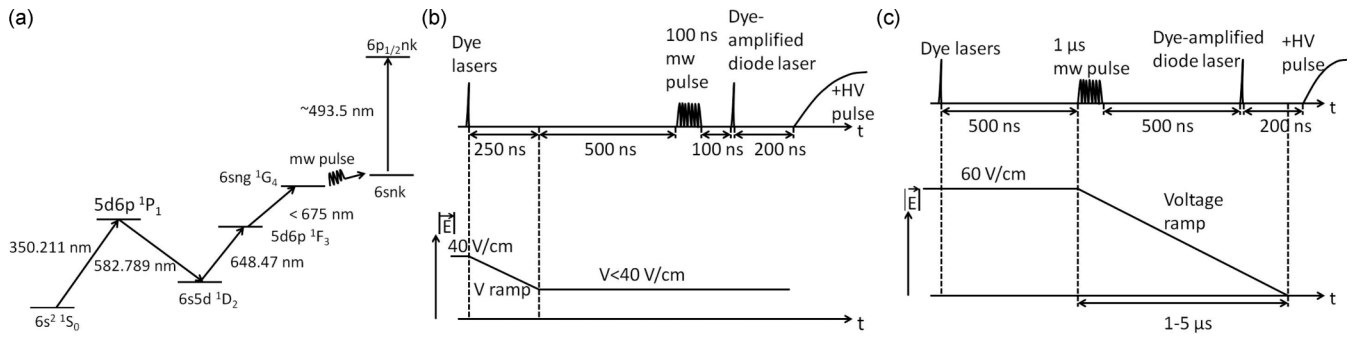

FIG. 2. (a) The energy levels. (b) In this timing sequence laser pulses 1, 2, 3, and 4 occur in a static field of 40 V/cm. The field is then reduced to the desired value in 250 ns; 500 ns later, a 100-ns pulse microwave is applied. The fifth laser is fired 100 ns after the microwave pulse. The positive high-voltage pulse is applied 200 ns later to collect the ions. (c) In this timing sequence laser pulses 1, 2, 3, and 4 occur in a static field of 60 V/cm; 500 ns later, the decreasing field ramp is started, and the 1-μs microwave pulse is applied at the same time. The slew rate of the field is adjusted to reach the desired values where the fifth laser is fired 500 ns after the microwave pulse. The positive high-voltage pulse is applied 200 ns later to collect the ions.

following way. The continuous-wave 10- to 20-GHz output of a Hewlett-Packard 83550A sweep oscillator is formed into 100-ns or 1-μs pulses by using a General Microwave DM862B switch. The microwave pulse is then frequency doubled twice, by a Phase One SX40-220 active doubler and a Pacific Millimeter V2WO passive doubler, respectively, to form a microwave pulse of 50–75 GHz. To produce a microwave frequency of 40–60 GHz, the microwave pulse from the microwave switch is quadrupled by a Narda-DBS active quadrupler. The 50–75-GHz pulse travels through WR15-19-28 waveguide adapters and the 40–60-GHz pulse travels through WR19-28 waveguide adapters to a section of WR28 waveguide which passes into the vacuum chamber and terminates in a WR28 microwave horn in front of the field plates. The lasers and microwaves are linearly polarized vertically, in the same direction as the static field, so we always have states of $|m| = 0$.

III. EXPERIMENTAL RESULTS AND DISCUSSION

A. Experimental results

We have observed the transitions from bound $6snk$ Stark states to the $6p_{1/2}nk'$ autoionizing Stark states in fields from 0 to 47 V/cm, as shown in Figs. 3 and 4. The power of the dye-amplified diode laser is attenuated so that the spectra are unsaturated. In Figs. 3 and 4 we show the spectra observed from the $6s17k$, $k = 6$ and $k = 10$ states in static fields from 0 to 47 V/cm. In Fig. 5 we show the transitions from different $6s17k$ states in the field of 16.67 V/cm. In zero field the $6p_{1/2}17$ ($\ell = 6$) spectrum exhibits two peaks at 20 261.871(10) and 20 261.959(10) cm^{-1}. When these photon energies are added to the $6s17$ ($\ell = 6$) energy of 41 654.876 cm^{-1} we obtain the term energies 61 916.747(10) and 61 916.835(10) cm^{-1}, as shown in Fig. 3. Since many of the spectra have been recorded in fields, they are most informative when plotted as final-state energies, and we follow this convention throughout the paper. The splitting of the $6p_{1/2}17(\ell = 6)$ state is 2.57(30) GHz,

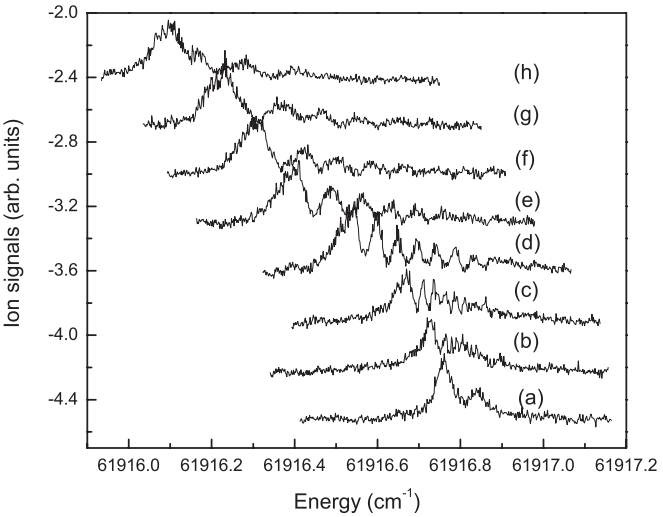

FIG. 3. The Ba $6s17k = 6$ state to $6p_{1/2}17k'$ states photoexcitation spectra in the electric fields of (a) 0, (b) 4.4, (c) 9.73, (d) 19.07, (e) 27.32, (f) 33.4, (g) 38.57, and (h) 47.23 V/cm. The horizontal axis is the final-state energy.

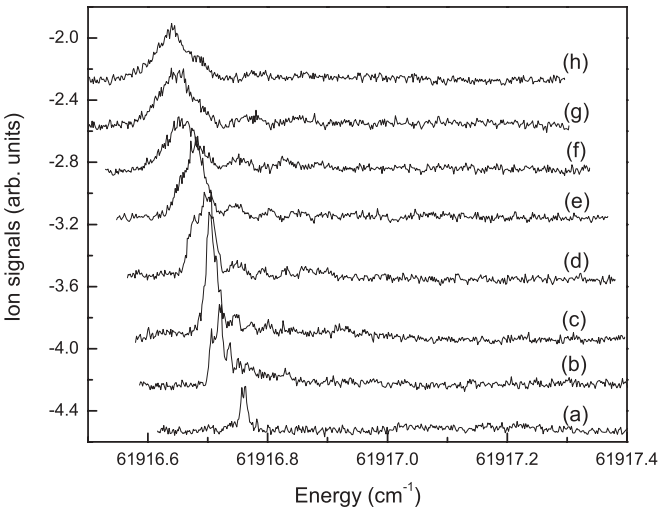

FIG. 4. The Ba $6s17k = 10$ state to $6p_{1/2}17k'$ states photoexcitation spectra in the electric fields of (a) 0, (b) 4.83, (c) 10, (d) 15, (e) 19.5, (f) 27.67, (g) 33.75, and (h) 39.17 V/cm. As in Fig. 3, the horizontal axis is given in terms of the final-state energy.

which is larger than the K splitting in the $6s17(\ell = 6)K$ state by a factor of 10. The hydrogenic level of the $6p_{1/2}17\ell$, $\delta_\ell = 0$, state is at 61 916.759 cm^{-1}. Hence, the low-energy peak of the $6p_{1/2}17(\ell = 6)$ is below the hydrogenic level, and the high-energy peak of the $6p_{1/2}17(\ell = 6)$ is above the hydrogenic level. It is the K splitting of Ba $6p_{1/2}17(\ell = 6)K$ states, where $K = \ell \pm 1/2$. This splitting produces the two values of quantum defects, 0.0003(2) and $-0.0017(2)$ for $K = 11/2$ and $13/2$, respectively. The average autoionization width of the Ba $6p_{1/2}17\ell$, $\ell = 6$ state is 0.045(10) cm^{-1} which agrees well with the value in Ref. [15] scaled to $n = 17$. The Ba $6p_{1/2}17\ell$, $\ell > 6$ states in zero field have small autoionization widths since the autoionization rate falls

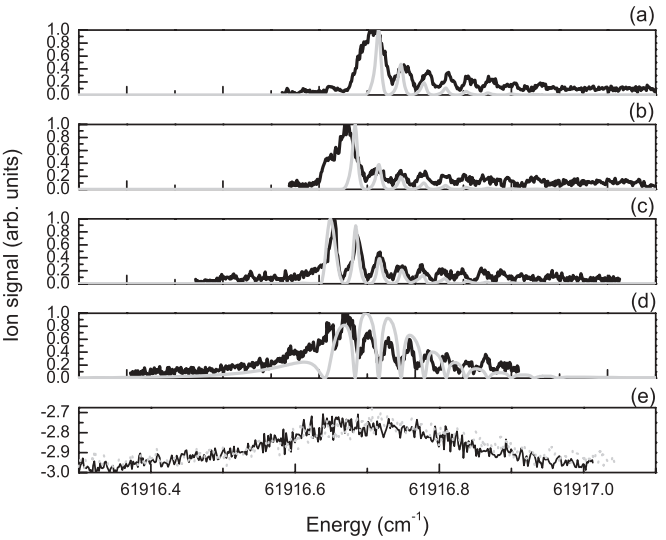

FIG. 5. The experimental (solid black lines) and calculated (solid gray lines) spectra of Ba $6p_{1/2}nk'$, $n = 17$ autoionizing states starting from the bound $6snk$ states of (a) $k = 9$, (b) $k = 8$, (c) $k = 6$, (d) $k = 5$ in 16.67 V/cm, and (e) $k = 5$, $K = 11/2$ (solid line) and $K = 9/2$ (dot line), in zero field.

exponentially with ℓ. The experimentally observed widths of the zero field of $6p_{1/2}17\ell$ states, $\ell > 6$, are $\sim$0.01 cm^{-1} which is the dye-amplified diode laser linewidth. Looking beyond the zero-field trace of Fig. 3 we see that the spectra in fields from 4.4 to 47.23 V/cm consist of a broad peak, which shifts from 61 916.75 cm^{-1} to 61 916.1 cm^{-1}, and satellite peaks on the high-energy side of the broad peak. The broad peak is due to the $6p_{1/2}17k'$ Stark state most similar to the $6snk$ state, and the shake-up satellite peaks on the high-frequency side are due to $6p_{1/2}17k'$ Stark states of higher k'.

At this point it is useful to expand upon our earlier description of ICE. In ICE of the Ba $6snk$ state to the $6p_{1/2}nk$ states the inner electron undergoes the Ba$^+$ $6s_{1/2}$-$6p_{1/2}$ transition while the outer electron's wave function is projected from the initial $6snk$ wave function onto the $6p_{1/2}nk'$ wave functions. This projection is represented by an overlap integral. If the two sets of Stark states are identical the initial $6snk$ wave function overlaps with only the $6pnk'$ wave function which is identical, and $k' = k$. All other overlap integrals are zero, and in this case the ICE spectrum consists of a single peak. If, on the other hand, the two sets of Stark states are not the same, there is more than one nonzero overlap integral, and satellite peaks appear in the ICE spectrum. The many satellite peaks visible in Figs. 3, 4, and 5 tell us that the two sets of Stark states are not identical. Since the $6snk = 6$ state is a red Stark state, its strongest ICE transition is to the $6p_{1/2}nk$ Stark state with a similar shift to lower energy with field, as seen in Fig. 3. The frequency of the transition to the broad peak remains close to the frequency of the Ba$^+$ transition at 20 261.561 cm^{-1}.

In Fig. 4 we show ICE spectra obtained starting from the $6s17k = 10$ state. We again see a broad peak, which moves only slightly with field, from 61 916.75 cm^{-1} to 61 916.65 cm^{-1} as the field is raised to 47.23 V/cm. Again we observe satellite peaks on the high-energy side of the strong broad peak. The broad peak is the transition to the $6p_{1/2}nk'$ state most similar to the bound $6snk = 10$ state. Both states have very small Stark shifts since they are near the centers of their respective Stark manifolds. The satellites on the high-frequency side of the broad peak are due to $6p_{1/2}nk'$ states of $k' > 10$. What is surprising is that no satellite transitions are observed to the lower-energy Stark states, only to the higher-lying Stark states. We only see higher-lying Stark states irrespective of which $6snk$ state we use as the starting point.

Figs. 3, 4, and 5 exhibit two prominent features. First, as shown particularly clearly by Fig. 3, the width of each peak increases as the electric field increases. Second, in fields below 20 V/cm each spectrum has one large peak and small satellite peaks only on the high-energy side of the large peak. For fields above 20 V/cm the higher-energy satellite peaks are suppressed in amplitude. Both of these features are due to the fact that the $6p_{1/2}nk$ Stark manifold changes character, although gradually, at fields of $\approx$20 V/cm. Specifically, for fields less than 20 V/cm the broad $6p_{1/2}17h$ state is not part of the manifold, and in this regime the $6p_{1/2}nk$ Stark manifold has one less state than the $6snk$ manifold. As a consequence the Stark states of the two manifolds are different. On the other hand, above 20 V/cm both manifolds have the same number of states, and they are similar. To further discuss the data, it is useful to introduce the idea of the incomplete Stark map and how it affects the overlap integrals.

B. Incomplete Stark manifolds and overlap integrals

1. Ba bound $6snk$ Stark states

In an electric field, the nk Rydberg Stark states are a linear combination of the zero-field $n\ell$ states. We find the $6snk$ Stark states' energies by diagonalizing the Hamiltonian

$$H = H_0 - Ez \tag{1}$$

using the zero-field $6sn\ell$ states as basis states. In Eq. (1) H_0 is the energy of the atomic state in zero field, $-1/2(n-\delta_\ell)^2$, where δ_ℓ is the quantum defect of the ℓ state and E is the field applied in the z direction. In the weak fields of interest here, ℓ is still a good quantum number for $\ell \leqslant 4$ due to their large quantum defects. Therefore, for $k \geqslant 5$ states, the contribution of the $\ell \leqslant 4$ states is negligible. In the calculation of an incomplete Stark map of $6snk$, the Hamiltonian matrix only contains states of one n and $\ell \geqslant 5$. Figure 6 shows the incomplete Stark map of the $m = 0$ $6snk$ states of $n = 17$ and $k \geqslant 5$ obtained by diagonalizing the $(n-5)\times(n-5)$ Hamiltonian. The diagonal terms are $-1/2(n-\delta_\ell)^2$, where δ_ℓ is the quantum defect of the ℓ state, and the off-diagonal matrix elements are $-E\langle n\ell|z|n\ell'\rangle$, for $\ell' = \ell \pm 1$.

2. Ba $6p_{1/2}nk$ Stark autoionizing states

In calculating the Stark effect of the Ba $6p_{1/2}n\ell$ autoionizing states we follow a similar procedure. We ignore the $6p_{1/2}n\ell$ states of $\ell < 5$ because of their large quantum defects. While the $6p_{1/2}nh$ state has a small quantum defect, we do not include it in the calculation of the Stark effect at low field

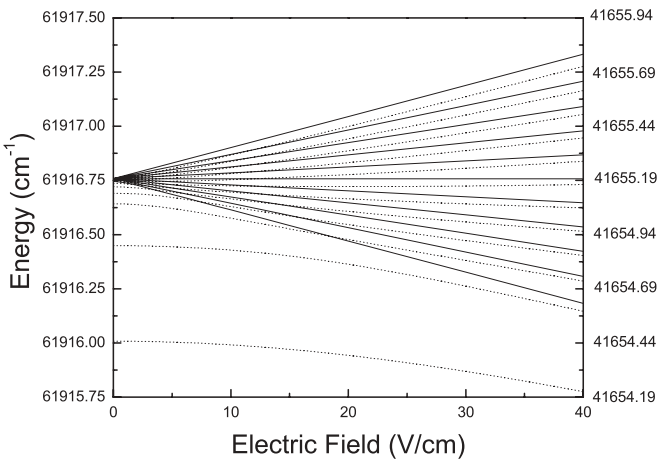

FIG. 6. The incomplete Stark map of the $6p_{1/2}17k'$ states (solid lines) and $6s17k$ states (dotted lines), $6 \leqslant k' \leqslant 16$ and $5 \leqslant k \leqslant 16$. The labeled axis on the left is the energy scale for the $6p_{1/2}17k'$ states, and the labeled axis on the right is the scale for the $6s17k$ states. Both left and right axes have the unit of energy (cm^{-1}). The graph indicates that the Rydberg electron wave functions of the bound $6s17k$ and of the autoionizing $6p_{1/2}17k$ are not well overlapped in low field. There is the probability that during ICE the Rydberg electron initially in the nk state will end up in states other than the nk state, leading to the shake-up satellites.

since its zero-field width overlaps all the higher ℓ states. We treat the $6p_{1/2}n\ell$ states as discrete states and diagonalize the Hamiltonian of Eq. (1). Therefore, the Hamiltonian matrix is $(n-6)\times(n-6)$. For the $6p_{1/2}17i$ state we use the observed quantum defect $\delta_{\ell=6} = 0.000\,3(2)$ in the calculation. In terms of Fig. 6, it corresponds to an energy of 61 916.75 cm^{-1}. The higher ℓ states lie between the $\ell = 6$ energy and the hydrogenic level, and therefore their quantum defects are less than the quantum defect of the $\ell = 6$ state. Thus, we use zero quantum defects for the $6p_{1/2}17\ell$, $\ell > 6$ states. The incomplete Stark map of $6p_{1/2}nk$, $n = 17$, $k \geqslant 6$ is shown in Fig. 6.

3. *Overlap integrals*

The probability that the Rydberg electron is shaken to the nk' state during ICE depends on the overlap integral between the Rydberg bound state (nk) and the Rydberg autoionizing state (nk'), $O(W_f) = \langle\psi_{nk}(W_i)|\psi_{nk'}(W_f)\rangle$, and the density of the final states, $D_f(W_f)$.

a. Identical manifolds. If the bound and autoionizing Rydberg manifolds are identical, that is, they contain the same number of ℓ states with the same quantum defects, the bound state overlaps with only one autoionizing Stark state, and there are no satellite peaks. The overlap integral yields a δ function.

b. Manifolds with identical quantum defects but different numbers of states. If, for each ℓ, the bound and autoionizing Stark states have the same quantum defects, but the autoionizing Stark manifold has one less ℓ state (no h state to be precise), then the overlap integral is a broadened δ function which is nonzero for few $k' \neq k$ states as shown in Fig. 7. In Fig. 7, we use hydrogen wave functions for both bound and autoionizing Stark states and only include $\ell \geqslant 5$ and $\ell \geqslant 6$ in the Hamiltonian of Eq. (1) for the bound and autoionizing Stark states, respectively. The broadening of the δ function is due to the fact that the two manifolds do not contain the same number of states but are otherwise identical.

c. Manifolds with the same number of states but nonidentical quantum defects. In this case the overlap integral is a slightly broadened δ function, as in case b.

d. Nonidentical manifolds with nonidentical quantum defects. Finally, we consider the case in which these Stark manifolds containing different numbers of ℓ states having different quantum defects in the two cases. As before, we use $\delta_\ell = 0.000\,3$ for the quantum defect of the $6p_{1/2}17i$ state and zero for all higher ℓ states and the positive quantum defects implied by Fig. 6 for the $6s17\ell$ states. The resulting overlap integral for the Stark states is shown in Fig. 8. The overlap integral is asymmetrically broadened to high k, which agrees with our experimental observations. Essentially the same result is obtained if the quantum defect of the $6p_{1/2}17i$ state is assumed to be zero. If we reverse the sign of each of the quantum defects of the $6s17\ell$ states, so that the energy-level structure of Fig. 6 is inverted, we find a reversal of the overlap integral,

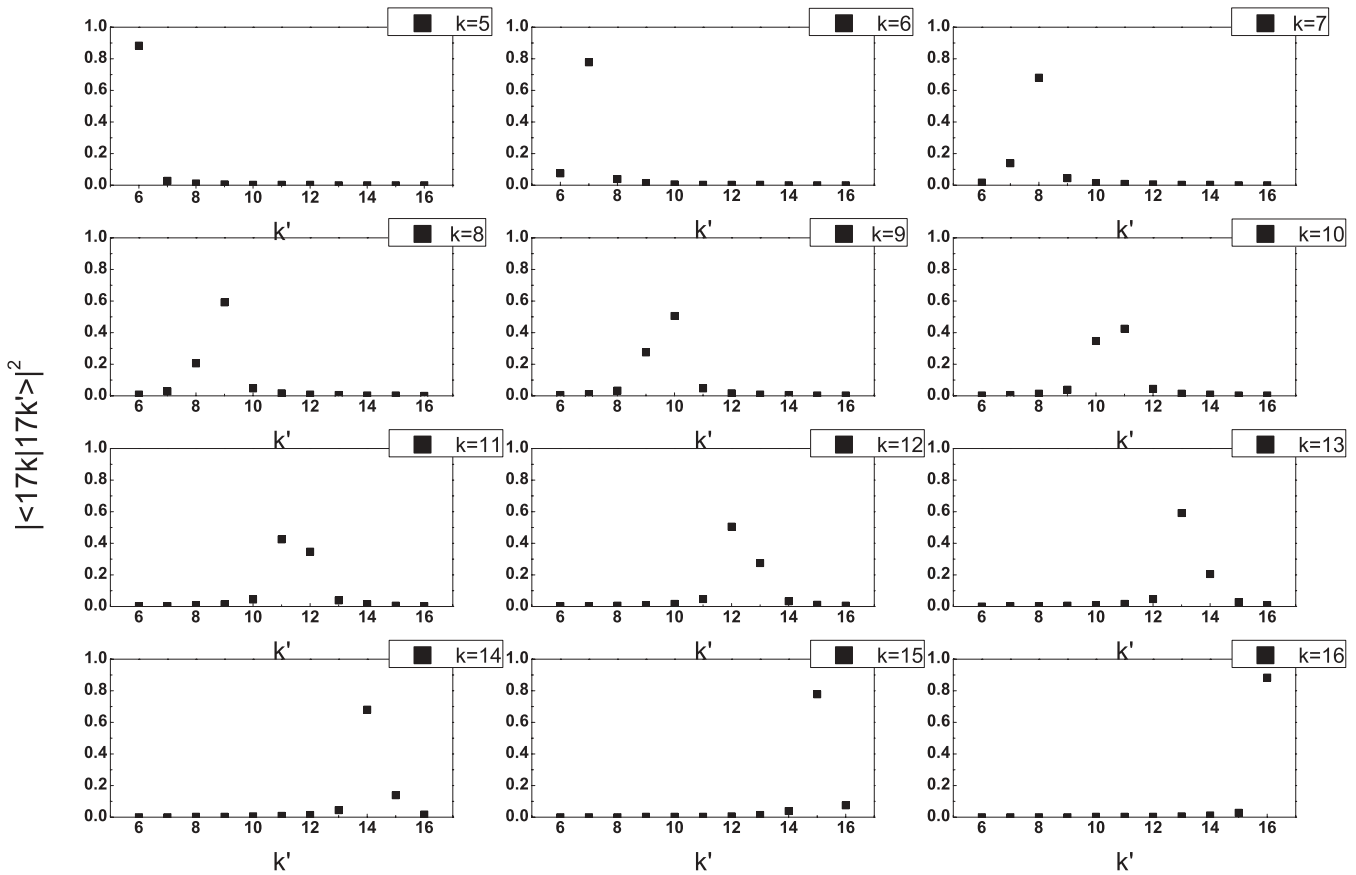

FIG. 7. The squared overlap integrals of the Rydberg electron wave functions of $6snk$ Stark state and $6p_{1/2}nk'$ Stark autoionizing state for different initial states k to all final k', $n = 17$, states at $E = 16.67$ V/cm. Here we use zero quantum defects to calculate both bound and autoionizing wave functions at $E = 16.67$ V/cm.

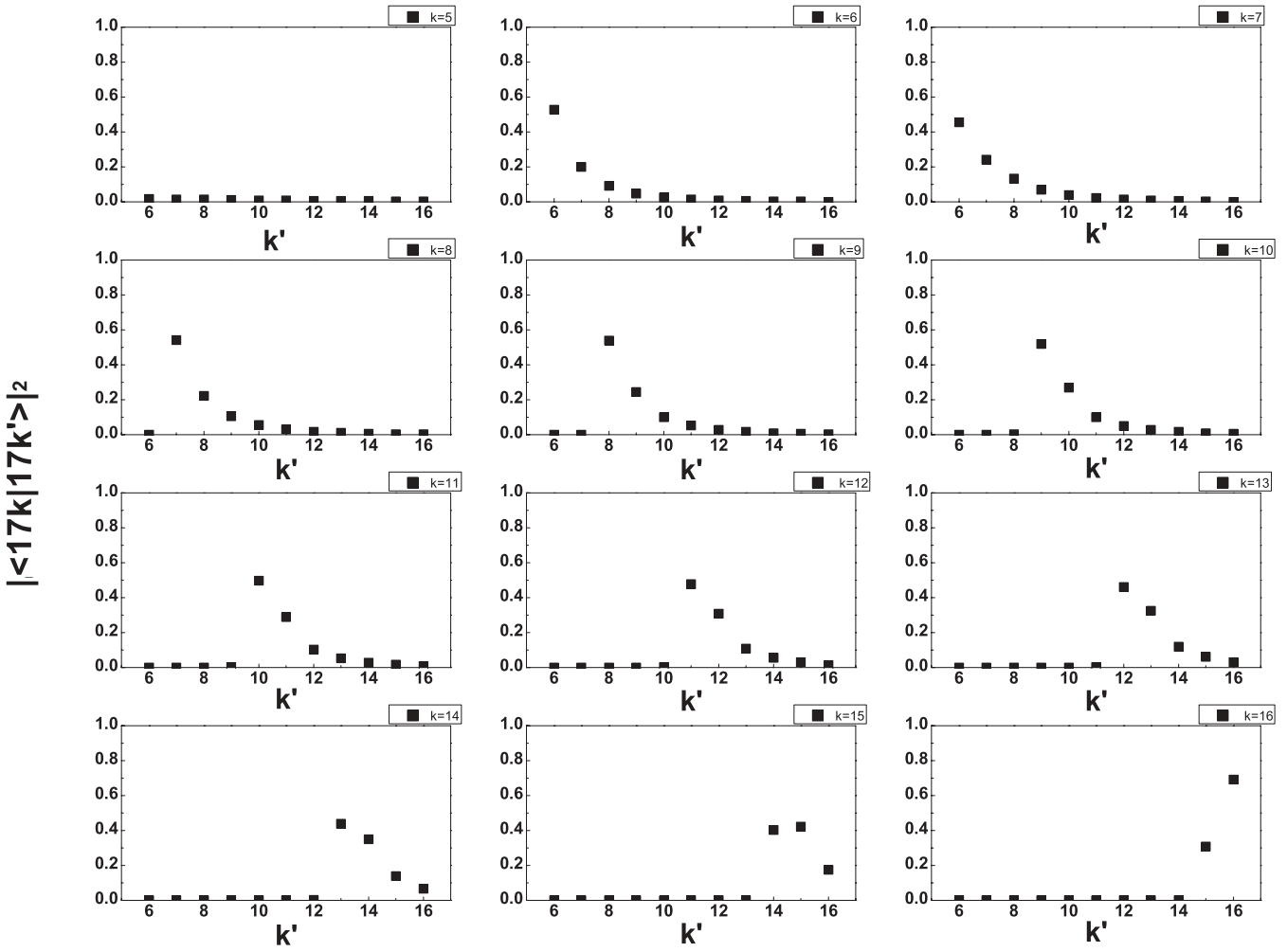

FIG. 8. The squared overlap integrals of the Rydberg electron wave functions of $6snk$ Stark state and $6p_{1/2}nk'$ Stark autoionizing state for different initial states k to all final k', $n = 17$, states at $E = 16.67$ V/cm.

as shown in Fig. 9. In short, whether the satellite structure occurs on the high- or low-energy side indicates the sign of the change in the quantum defects between the $6sn\ell$ and $6p_{1/2}n\ell$ states.

The quantum defects of the high-ℓ $6sn\ell$ and $6p_{1/2}n\ell$ states are different because the polarizabilities of the Ba^+ $6s$ and $6p_{1/2}$ states are different. The asymmetric shake-up satellites are thus a reflection of the change in the polarizability of the ionic core. This observation is not the first observation of changes in the shake-up satellites due to changes in the polarizability of the ionic core. Eichmann *et al.* observed an asymmetry in red and blue shake-up satellites in the ICE to double Rydberg states of Sr due to the much larger polarizability of the highly excited ionic core [16]. While the manifestation is different, the cause is the same.

In our case the two Stark manifolds are clearly not the same in fields less than 20 V/cm. In particular, the bound $6snk$ manifold consists of $\ell \geqslant 5$ states while the autoionizing $6p_{1/2}nk$ manifold consists of $\ell \geqslant 6$ states. The overlap integrals for different initial states k to all final k' in the field of 16.67 V/cm, $n = 17$, states are shown in Fig. 8. Figure 8 suggests that the initial $6snk$ states, $k > 6$, are most likely to make a transition to $6p_{1/2}nk_{\rm min}$ final states, with $k_{\rm min} = k - 1$, and the $6snk = 6$ state is most likely to make a transition to $6p_{1/2}nk_{\rm min} = 6$. As the field increases, the spread in energy of the Stark manifold increases. When the extent of the Stark manifold is greater than the autoionization width of the autoionizing h state, the h state becomes part of the manifold. The numbers of states in the manifolds of the bound and autoionizing states are the same and the manifolds are more similar than in the low field. Hence, $k_{\rm min}$ will change from $k_{\rm min} = k - 1$ to $k_{\rm min} = k$. The spread in energy of the Stark manifold of $k > 5$ states is equal to the autoionizing width of the $6p_{1/2}17h$ state at $E = 12.5$ V/cm. Hence, a field substantially stronger than 12.5 V/cm is required for the h state to fully become part of the manifold. In the calculation of the autoionizing spectra, we assume that field is low enough that the h state is not part of the manifold. From Fig. 8 the cross sections to $k' < k_{\rm min}$ are negligible. This surprising feature derives from the fact that both the $6snk$ wave functions and the $6p_{1/2}nk'$ wave functions are the eigenvectors of incomplete and different Stark manifolds, and it agrees well with the experimental data from Figs. 3, 4, and 5. It is independent of the quantum defect values as long as the quantum defect decreases monotonically as ℓ increases.

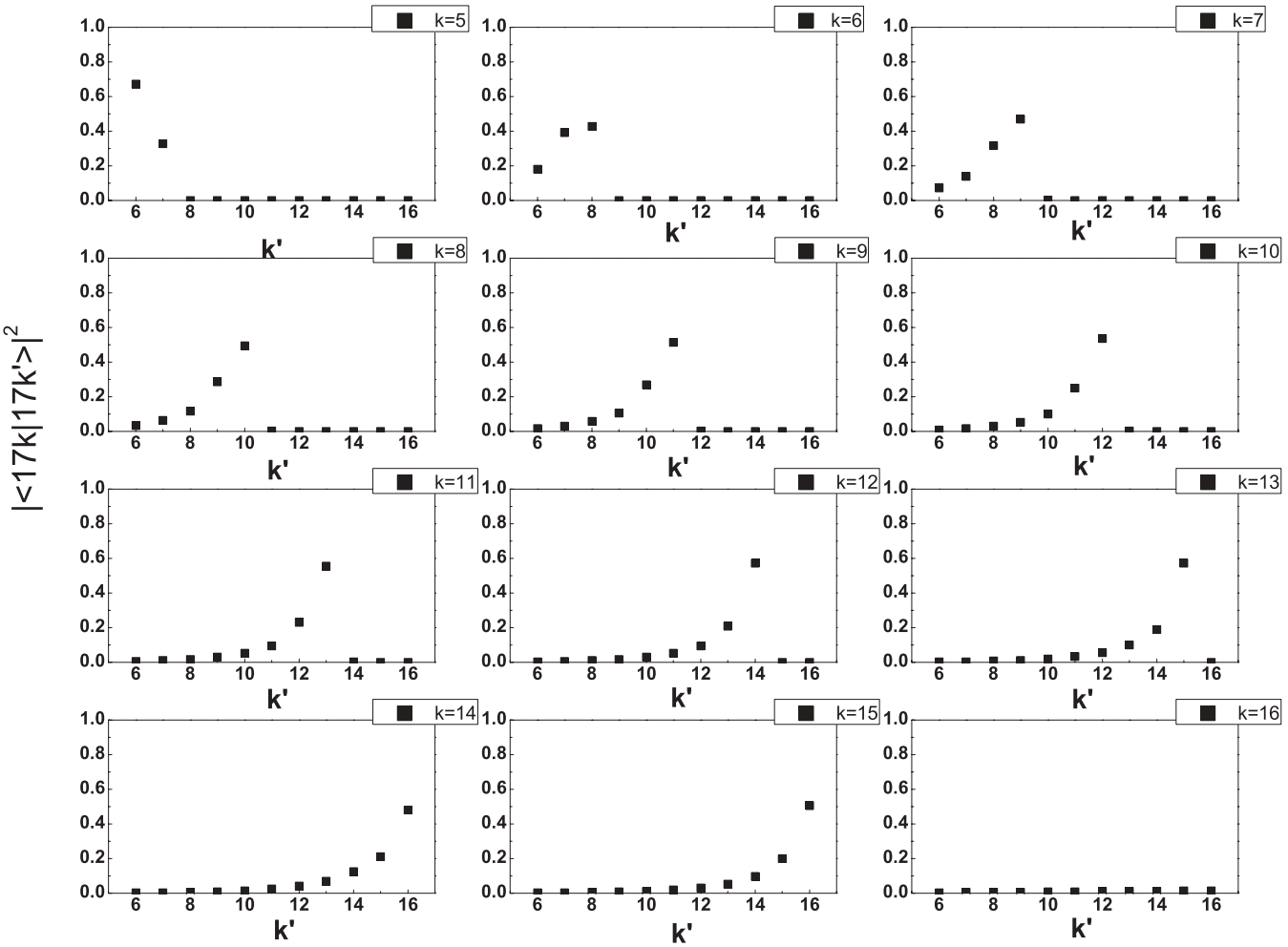

FIG. 9. The squared overlap integrals of the Rydberg electron wave functions of $6snk$ Stark state and $6p_{1/2}nk'$ Stark autoionizing state for different initial states k to all final k', $n = 17$, states at $E = 16.67$ V/cm. The quantum defects of the bound states have the opposite signs to the values used to calculate Fig. 8.

C. Discussion

1. Autoionization widths of Ba $6p_{1/2}(n = 17)k'$ states in low electric field

The overlap integrals provide the information about the final states nk' of the Rydberg electron. With this information, we can correctly assign k' to each peak. We fit Lorentzian functions to the largest, the lowest-energy, peaks of the graphs from Figs. 3 and 4, yielding the autoionization widths of the $6p_{1/2}17k'$ states as a function of the electric field as shown in Fig. 10.

The observed variation of the observed widths of Fig. 10 with field is due to the varying composition of the states with field. In Fig. 11 we plot the widths for each of the states shown in Fig. 10 with the calculated widths, shown as broken lines. The calculated width at any field is the average of all the ℓ states contained in the manifold at that field. It changes in steps at the fields where progressively lower ℓ states join the manifold. We use as a criterion that the energy spread of the manifold is equal to the autoionization width of the lower ℓ state which is joining the manifold. This field is slightly larger than $E \simeq 2\delta_g/3n^5$. The steps at 1.67, 12.5, 80.8, and 481 V/cm are where the $6p_{1/2}17\ell$ states of $\ell = 6$, 5, 4, and 3, respectively, join the manifold. The autoionization widths in zero field used in the calculation are from Ref. [15].

In the field, for Ba $6p_{1/2}17k'$, $k' > 6$ states, the autoionization widths are almost the same for all k' at any electric field. The widths increase as the field increases because, for each $k' > 6$ state, $\ell \leqslant 6$ character is mixed in, and the width broadens. Having to share its width with other high-k' states, the autoionization width of the $6p_{1/2}nk'$, $k' = 6$ state falls from its zero-field value to roughly $A_A(nk') = \frac{A_A(n\ell=6)}{n-5} = 0.005$ cm^{-1} at $E = 1.67$ V/cm. Here $A_A(nk')$ and $A_A(n\ell)$ are the autoionization widths of the Ba $6p_{1/2}nk'$ and $6p_{1/2}n\ell$ states, respectively. At the field $E = 12.5$ V/cm, where the spread of the Stark states $k' \geqslant 6$ is equal to the autoionization width of the h state, the average autoionization rate of the states in the manifold increases and it is equal to $A_A(nk') = \sum_{\ell=5}^{n-1} A_A(n\ell)/(n-4)$. In practice the widths do not follow the step-function behavior shown in Fig. 11 but it is clear that the general trends of the observed widths match the steps. To calculate the autoionization widths in detail, one must take into account of the interaction between discrete states, the

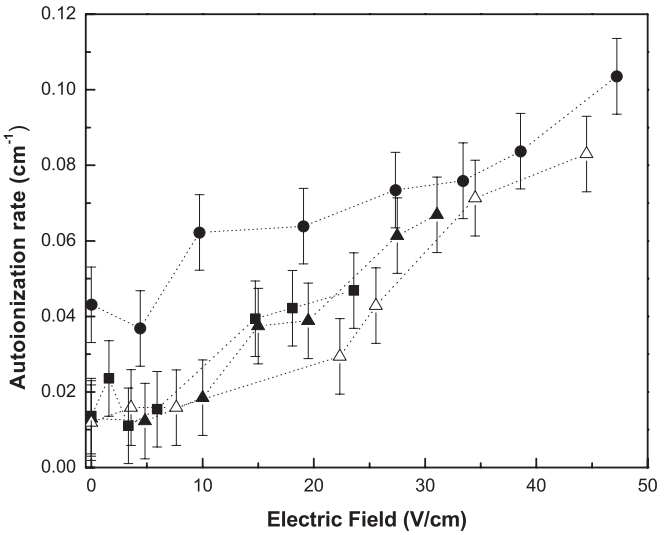

FIG. 10. The autoionization widths of the Ba $6p_{1/2}17k'$ states for $k' = 6$ (●), 8 (■), 9 (▲), and 11 (△) as a function of electric field. The widths increase as the electric field increases due to the increasing admixture of the low ℓ states, $\ell < 5$, which have not yet joined the Stark manifold.

true continuum and the quasicontinua of $\ell = 3$, 4, and 5. The result should yield the smooth curve that increases with the field, more or less following the steps of Fig. 11.

2. *Autoionization spectra of Ba $6p_{1/2}nk$ in low electric field*

One of the surprising features of Figs. 3, 4, and 5 is the presence of satellite peaks only on the high-energy side of the main peak. With this thought in mind it is useful to reexamine Fig. 5, the ICE spectra from several $6snk$ states in a field of 16.67 V/cm. The shake-up satellite features at the locations of the Stark states above the one principally excited are quite evident, and they have the expected spacing, 0.045(10) cm^{-1}. An important feature is that in the spectra obtained from the $6snk$ states of $k > 5$ all the shake-up satellite features occur at the same energies, which correspond to the energies of the $6p_{1/2}nk'$ states. In contrast, in the ICE spectrum from the $6snk$ $k = 5$ state the satellite features are shifted in energy so that the peaks are approximately midway between the locations of the peaks in the other ICE spectra of Fig. 5. This observation is unique in ICE spectra.

A qualitative explanation of the spectra of Fig. 5 is that the bound $6snk$ states are linear combinations of $\ell \geqslant 5$ states, all of which are discrete. In this field the $6p_{1/2}nh$ state is broad, effectively a continuum, as shown in Fig. 5, and the quasidiscrete Stark states are composed only of $\ell \geqslant 6$ states. The observed autoionization widths in zero field of $6p_{1/2}n\ell$, $n = 17$ and 18, $\ell = 5$ and 6 are given in Table I. Thus in the excitation from a bound $6snk$ state, excitation to both the discrete $6p_{1/2}nk$ Stark states and the $6p_{1/2}nh$ continuum can occur. For high k the latter is suppressed, but for excitation from the $6snk$ $k = 5$ state both are important, leading to the observed shift of the satellite peaks.

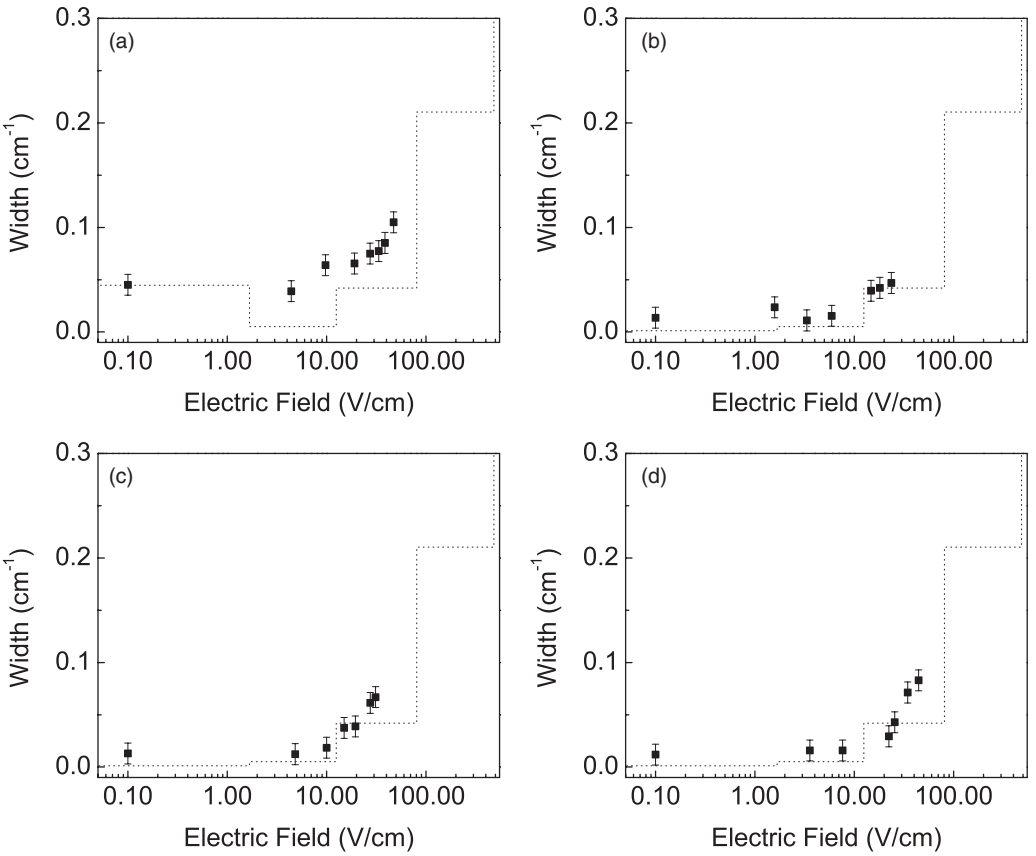

FIG. 11. The observed (■) and calculated (dotted line) widths as a function of the electric field for the Ba $6p_{1/2}17k'$, (a) $k' = 6$, (b) $k' = 8$, (c) $k' = 9$, and (d) $k' = 11$.

TABLE I. The observed autoionization width of the $6p_{1/2}n\ell$ states.

n	$\ell = 5$ (cm^{-1})	$\ell = 6$ (cm^{-1})
17	0.35(1)	0.045(10)
18	0.26(1)	0.024(20)

The above picture is essentially Fano's configuration interaction picture, with one continuum and many discrete levels embedded in the continuum as shown in Fig. 12 [17]. The $6p_{1/2}nh$ state has a finite Lorentzian profile, but we assume it to be a true continuum. The discrete states, the Stark states composed of the $6p_{1/2}n\ell$ states of $\ell > 5$, interact with the continuum via fraction of h mixing into each discrete state due to the electric field. As the energy passes through each discrete state the continuum phase is shifted by π. The discrete states are broadened by the continuum and acquire width of $\Gamma = 2\pi|V_W|^2$ where V_W is the coupling from the discrete state to the continuum.

The photoexcitation cross section from the initial state $6snk$ to the final state $6p_{1/2}nk'$ can be written as

$$\sigma_{6snk\to 6p_{1/2}nk'} \propto |\langle 6s|\mu|6p_{1/2}\rangle\langle\psi_{nk}|\psi_{nk'}\rangle|^2, \tag{2}$$

where $\psi_{nk'}$ is the eigenstate of the discrete-continuum configuration and normalized per unit energy. The Ba initial bound state $6snk$ Rydberg electron wave function can be written as

$$\begin{aligned}\psi_{nk} &= \sum_{\ell} a_{k\ell}\psi_{n\ell} \\ &= a_{kh}\psi_{nh} + \sum_{\ell=6}^{n-1} a_{k\ell}\psi_{n\ell}.\end{aligned} \tag{3}$$

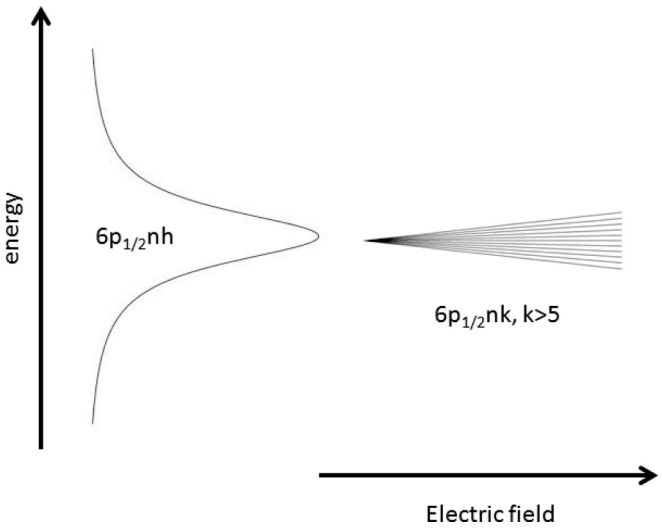

FIG. 12. A simple model of the problem. The discrete levels embedded in the continuum have finite energy widths due to the coupling to the continuum, which leads to interference between the excitation amplitudes to the continuum and the discrete states. As a result, the excitation spectra to the same final energy are very different for different initial states.

The Ba autoionizing state $6p_{1/2}nk'$ Rydberg electron wave function can be written as

$$\begin{aligned}\psi_{nk'} &= \sum_{\ell} a'_{k'\ell}\psi_{n\ell} \\ &= \varphi_{\rm con} + \sum_{\ell=6}^{n-1} a'_{k'\ell}\psi_{n\ell}.\end{aligned} \tag{4}$$

The first term of Eq. (4) is the $6p_{1/2}17h$ continuum due to its large autoionization width. The second term is the discrete state. In the presence of an electric field the continuum has phase shifts at the resonances, and the discrete states are broadened. We can express $\psi_{nk'}$ as [13,17,18]

$$\psi_{nk'}(W) = \int dW' b_{W'}\varphi_{W'} + A(W)\psi_{{\rm dis}_{nk'}}, \tag{5}$$

where $|A|^2$ is the spectral density of the autoionizing state $6p_{1/2}nk'$. In Fano's theory $|A|^2$ is a Lorentzian which comes from the bound-continuum coupling. Here we have simply used the observed $|A|^2$ values, which correspond to Lorentzian widths of 0.014 cm^{-1}. The discrete wave functions, $\psi_{{\rm dis}_{nk'}}$, are normalized per unit state and the continuum wave function, φ_W, is normalized per unit energy. The orthonormalization condition for $\psi_{nk'}$ is

$$\begin{aligned}\langle\psi_{nk'}(\bar{W})|\psi_{nk'}(W)\rangle &= A^*(\bar{W})A(W) + \int dW' b_{W'}(\bar{W})b_{W'}(W) \\ &= \delta(\bar{W} - W).\end{aligned} \tag{6}$$

Following Fano's theory and Ref. [13], the cross section from Eq. (2) becomes

$$\begin{aligned}\sigma_{6snk\to 6p_{1/2}nk'} \propto \big|\langle 6s|\mu|6p_{1/2}\rangle\big[a_{kh}\langle\psi_{nh}|\varphi_W\rangle\cos(\phi_{\rm con}+\gamma) \\ + A\langle\psi^b_{nk}|\psi_{{\rm dis}_{nk'}}\rangle\big]\big|^2,\end{aligned} \tag{7}$$

where ϕ is the phase shift of the continuum and the constant phase, γ, is defined as the radial phase difference between the initial state and the unperturbed continuum [13]. The first term has the Lorentzian profile modulated by the cosine of the phase shift. The continuum profile, the first term in the brackets of Eq. (7), is shown in Fig. 13(a). The second term in the brackets of Eq. (7) contains the overlap integral of the bound state ψ^b_{nk} and autoionizing discrete state $\psi_{{\rm dis}_{nk'}}$. The overlap integrals yield discrete values at different k values as shown in Fig. 8. We assign the same width to each point on the graphs in Fig. 8, yielding smooth curves through the points. With the observed $|A|^2$ values, overlap integrals, and positions of discrete states, we can plot the discrete profile, the second term in the brackets of Eq. (7), as shown in Fig. 13(b). The cross-section profile is the sum of the perturbed continuum, Fig. 13(a), and discrete profiles, Fig. 13(b), squared. We use Eq. (7) to fit our experimental data by letting γ be a variable to obtain the best fit. We determine the value of γ to be 3.05(20) radian.

As shown in Fig. 5, the calculated spectra reproduce one of the more prominent features of the experimental spectra, the phase shift of the satellite peaks seen in the excitation from the $6s17k = 5$ state shown in Fig. 5(d). However, the agreement is not complete. There are many factors that could contribute to the discrepancies between the experimental and calculated spectra. We have ignored the true continua in our configuration

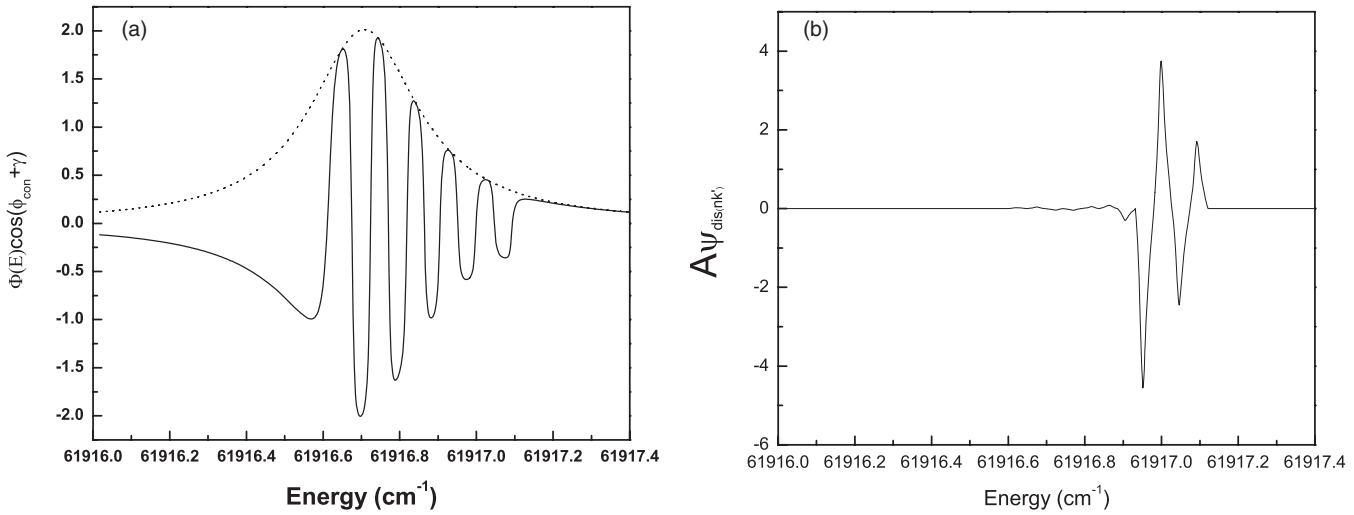

FIG. 13. (a) The excitation amplitudes to the perturbed continuum profile (solid line) and continuum profile (dotted line) of the Ba $6p_{1/2}nh$ autoionizing state, $\Phi_{\rm mod} = \Phi_{\rm con}\cos(\phi_{\rm con} + \gamma)$ with $\gamma = 0$. (b) The excitation amplitude to the discrete profile $A\psi_{{\rm dis}_{nk'}}$, starting from $6snk$, $n = 17, k = 14$.

interaction. For a correct treatment, the true continua, the continuum with the finite lifetime (the $6p_{1/2}nh$ state), and the discrete states must all be taken into account. The true continua are coupled to the continuum with the finite lifetime and the discrete states by the electron-electron interaction, $1/r_{12}$. Ignoring the true continua leads to an incomplete picture of the configuration interaction and contributes to the discrepancy between the theoretical predictions and the observations. One can use multichannel quantum defect theory (MQDT) to treat this problem, but it is a very complex many-channel problem. Nonetheless, we hope these data will inspire a theorist to take on the problem.

IV. CONCLUSION

We have observed the autoionization widths of the Ba autoionizing states $6p_{1/2}17k$, $5 \leqslant k \leqslant n-1$, in a low-electric-field regime. In general, the observed autoionization width increases as the electric field increases, and they agree well with the theoretical predictions. In the ICE spectra from the $6s17k$ to $6p_{1/2}17k'$ autoionizing states in electric fields less than 20 V/cm we only observe $k' \geqslant k-1$ for $k > 6$ and $k' \geqslant k$ for $k = 6$ shake-up satellites; $k' < k-1$ for $k > 6$ and $k' < k$ for $k = 6$ satellites are never observed, in agreement with our model based on an incomplete Stark manifold. The observed spectra can be explained by Fano's configuration interaction theory of one continuum ($6p_{1/2}nh$ state) with finite lifetime and multiple discrete states $6p_{1/2}nk$, $k > 6$ embedded in it.

ACKNOWLEDGMENTS

This work has been supported by the US Department of Energy, Office of Basic Energy Sciences. It is a pleasure to acknowledge useful discussion with R. R. Jones and V. Vorapipat.

[1] D. J. Armstrong and Chris H. Greene, Phys. Rev. A **50**, 4956 (1994).
[2] R. R. Jones, B. J. Lyons, M. A. Baig, Svetlana T. Djambova, and T. F. Gallagher, Phys. Rev. A **62**, 033408 (2000).
[3] J. B. M. Warntjes, F. Robicheaux, and L. D. Noordam, Phys. Rev. A **62**, 033407 (2000).
[4] F. Robicheaux, Phys. Rev. A **62**, 033406 (2000).
[5] V. L. Jacobs, J. Davis, and P. C. Kepple, Phys. Rev. Lett. **37**, 1390 (1976).
[6] A. Muller, D. S. Belic, B. D. DePaola, N. Djuric, G. H. Dunn, D. W. Mueller, and C. Timmer, Phys. Rev. Lett. **56**, 127 (1986).
[7] K. LaGattuta and Y. Hahn, Phys. Rev. Lett. **51**, 558 (1983).
[8] K. LaGattuta and Y. Hahn, J. Phys. B **15**, 2101 (1982).
[9] W. A. Chupka, J. Chem. Phys. **98**, 4520 (1993).
[10] E. W. Schlag, *ZEKE Spectroscopy* (Cambridge University Press, Cambridge, 1998).
[11] W. E. Cooke, T. F. Gallagher, S. A. Edelstein, and R. M. Hill, Phys. Rev. Lett. **40**, 178 (1978).
[12] N. H. Tran, P. Pillet, R. Kachru, and T. F. Gallagher, Phys. Rev. A **29**, 2640 (1984).
[13] U. Eichmann, T. F. Gallagher, and R. M. Konik, Phys. Rev. Lett. **90**, 233004 (2003).
[14] S. Gerstenkorn, P. Luc, and J. Verges, *Atlas Du Spectre D'Absorption De La Molecule D'iode* (Centre National De La Recherche Scientifique, Cedex, France, 1993).
[15] R. R. Jones, Ph.D. thesis, University of Virginia, 1990.
[16] U. Eichmann, V. Lange, and W. Sandner, Phys. Rev. Lett. **68**, 21 (1992).
[17] U. Fano, Phys. Rev. **124**, 1866 (1961).
[18] W. E. Cooke and C. L. Cromer, Phys. Rev. A **32**, 2725 (1985).